



**Transparent embedded Cu/Au-nanomesh electrode on flexible polymer film substrates**

Journal:	<i>RSC Advances</i>
Manuscript ID	RA-ART-05-2016-012054.R2
Article Type:	Paper
Date Submitted by the Author:	27-Aug-2016
Complete List of Authors:	Jung, Pil-Hoon; Korea university, Materials Science and Engineering Kim, Yang-Doo; Korea university, Materials Science and Engineering Choi, Hak-jong; Korea university, Materials science and engineering Sung, Young Hoon; Korea university, Materials Science and Engineering Heon, Lee; Korea university, Materials science and engineering
Subject area & keyword:	Nanomaterials applications < Nanoscience



## ARTICLE

## Transparent embedded Cu/Au-nanomesh electrode on flexible polymer film substrates

P.-H. Jung,<sup>a</sup> Y. D. Kim,<sup>a</sup> H.-J. Choi,<sup>a</sup> Y. H. Sung<sup>a</sup> and H. Lee<sup>a</sup>

Received 00th January 20xx,  
Accepted 00th January 20xx

DOI: 10.1039/x0xx00000x

www.rsc.org/

Transparent embedded copper/gold (Cu/Au)-nanomesh electrodes are promising candidates to replace indium tin oxide (ITO). They are fabricated on a polyethylene terephthalate (PET) flexible polymer film using a transfer process on the scale of 11 mm x 11 mm. Because of the oxidation of copper, Cu-nanomesh electrodes have very low electrical conductivity. In order to solve this problem, we fabricated an electrode using a Cu/Au-bilayer. With the bilayer, we obtained a high transmittance and electric properties at wavelengths of 400 nm–800 nm. Moreover, by controlling the pressure process, we obtained the transferred and embedded metal electrodes. We found that both the optical transmittance and the electrical conductivity of the embedded metal electrode were preserved after 50,000 bending cycles. Consequently, embedded Cu/Au-nanomesh electrodes have good mechanical strength and electrical properties appropriate for flexible transparent electrodes.

### 1. Introduction

In recent years, novel display products based on flexible components rather than conventional rigid-type panels—for example, smart watches, e-books, and high-end tablet PCs—have received significant attention for being more convenient, interesting, and easier to store.<sup>1,2</sup> It is believed that the market for flexible displays will expand rapidly. A transparent electrode is an essential element in optoelectronic devices, such as liquid-crystal displays (LCDs), solar cells, and organic light-emitting diodes (OLED), and offers current spread and optical in- and out-coupling.<sup>3–6</sup> Metal oxide-based materials, such as indium-zinc oxide (IZO), ITO, and aluminum-zinc oxide (AZO), have been widely used for transparent electrodes.<sup>7–12</sup> Even though ITO has superior properties, such as high optical transparency and electrical conductivity, the application of metal oxide-based materials in flexible devices is limited because of their high deposition temperatures, high cost, brittleness, and susceptibility to conductivity changes if subject to bending.<sup>13,14</sup>

Therefore, there have been many approaches to replace conventional ITO in order to achieve flexible substrates. For instance, conducting polymers,<sup>15–17</sup> carbon nanotubes,<sup>18–20</sup> graphene,<sup>21,22</sup> copper fibers,<sup>23</sup> and other nanostructures have been widely explored. Although carbon nanotubes are actively studied by a large number of research groups, their electrical conductivity has not been sufficiently high until now for the fabrication of organic

devices because of the remaining high contact resistance among the tubes.<sup>24–26</sup> Kim et al. have studied graphene films with high transparency above 80% combined with superior mechanical strength and a sheet resistance of 50  $\Omega$ /sq, which was realized using chemical vapor deposition (CVD) in the sample preparation. However, the production cost is high because the CVD process requires high temperatures greater than 1000 °C.<sup>27–29</sup>

In general, conducting polymers have been investigated to replace ITO electrodes. Even though these polymers are cost effective and flexible, conducting polymers such as poly(3,4-ethylenedioxythiophene-poly(styrenesulfonate))PEDOT:PSS exhibit lower electrical conductivity at the same light transmittance compared to metal oxide-based materials. In addition, depositing transparent thin films using conducting polymers on large-scale substrates demands post annealing, which implies high temperature and an additional reduction process. Unlike the other candidates mentioned above, metal structures using a copper/gold (Cu/Au) nanomesh represent an attractive material to replace ITO because both the electrical and optical properties are close to those of ITO.<sup>30,31</sup>

This paper introduces a novel method for fabricating a Cu/Au-nanomesh embedded in a polymer substrate with a large area, which increases the resistance against bending stress. To compare the stability against the bending stress, a transferred Cu/Au-nanomesh on a polymer substrate was also fabricated using nanotransfer printing based on partial pressure. Then, we confirmed that the transmittance and sheet resistance were >80% and <50  $\Omega$ /sq, respectively, for all Cu/Au-nanomesh electrode and investigated the difference in surface morphology between the transferred and embedded Cu/Au-nanomesh electrodes. We also confirmed their stability in a bending test of 50,000 cycles. Finally, we were able to demonstrate that the embedded Cu/Au-nanomesh

<sup>a</sup> Department of Materials and Science Engineering, Korea University, 5-1 Anam-dong, Sungbuk-Gu, Seoul 136-701, Republic of Korea.

† Footnotes relating to the title and/or authors should appear here.

Electronic Supplementary Information (ESI) available: [details of any supplementary information available should be included here]. See DOI: 10.1039/x0xx00000x

ARTICLE

Journal Name

is more stable than the transferred Cu/Au-nanomesh for bendable devices.

## 2. Experimental

### 2.1 Preparation

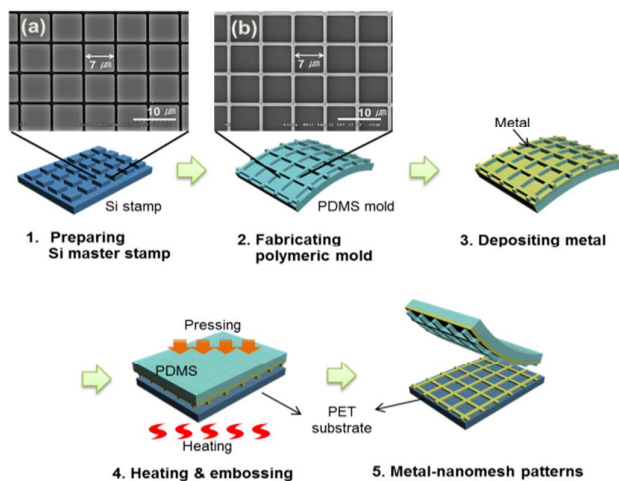


**Figure 1.** Schematic of the fabrication of metal-nanomesh patterns on a PET substrate.

The overall fabrication process for metal-nanomesh electrode patterns is shown in Figure 1. First, a Si master template was fabricated using conventional photolithography and reactive ion etching (RIE).<sup>32</sup> The silicon master stamp had a square-shaped array of Si patterns that were 7 μm in size, which included grooves of 500 nm in length with a 7.5 μm period (Fig. 1a). Prior to mold replication, the surface of the master stamp was coated with a hydrophobic self-assembled monolayer (SAM) for easier detachment of the polydimethylsiloxane (PDMS) mold. To coat the SAM monolayer, the Si master stamp was dipped into a heptadecafluoro-1,1,2,2-tetrahydrodecyl-trichlorosilane (HDFS)-based solution diluted with hexane at a 1:1000 ratio and stirred for 10 min. Then the Si master stamp was alternatively rinsed by hexane and deionized water and was dried with N<sub>2</sub> gas flow. The PDMS mold was prepared by pouring a mixture of Sylgard™ 184 resin and the curing agent (10:1 ratio) over the Si master stamp. After pouring the PDMS resin over the Si master stamp, the PDMS resin was placed in a low vacuum for half an hour to remove any air bubbles trapped in the PDMS. Then, the PDMS was heated at 80°C for 2 h to cure. Figure 1(b) shows the pattern of the cured PDMS mold, which is the reverse of the master stamp pattern. The PDMS mold of nanomesh-pattern had a line width and a line pitch of 500 nm and 7.5 μm, respectively. Afterward, metal was deposited on the PDMS mold by thermal evaporation. To fabricate the Cu-nanomesh electrode, the PDMS mold was deposited Cu layer of 150 nm thickness. Likewise, Cu/Au-nanomesh electrode was fabricated using deposited PDMS mold with Au/Cu bilayer of 50 nm/100 nm thickness.

### 2.2 Fabrication of metal-nanomesh electrode

The metal-deposited PDMS mold was uniformly placed over a polyethylene terephthalate (PET) substrate, and the metal-deposited PDMS mold and PET substrate were heated to 100 °C for 5 min and pressed at 0.5 to 4 bar to control the transfer process and the embedding process. After heating for 10 min and cooling to

room temperature, the metal-deposited PDMS mold was detached from the PET substrate. Subsequently, the transferred and embedded metal-nanomesh electrodes were formed on the PET substrate according to the pressure. Also, we can fabricate the Cu-nanomesh electrode and Cu/Au-nanomesh electrode using deposited PDMS with a Cu layer of 150 nm thickness and Cu/Au layer of 100 nm/50nm thickness, respectively.

## 3. Results and discussion

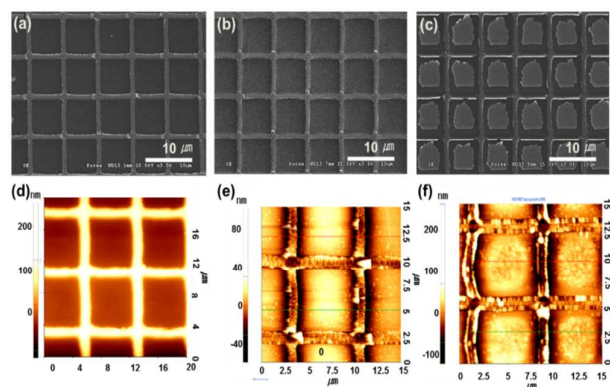


**Figure 2.** SEM images and AFM images of metal-nanomesh patterns on PET substrates fabricated with (a), (d) 0.5 bar, (b), (e) 2 bar, or (c), (f) 5 bar of pressure.

Figures 2(a)–(c) show SEM images of Cu-nanomesh electrodes on PET substrates. The height of the Cu-nanomesh electrode was measured by AFM, as shown in Figs. 2(d)–(f). The transferred Cu-nanomesh electrode was fabricated with 0.5 bar of pressure during processing, as confirmed by the SEM and AFM images. However, the SEM and AFM images in Figs. 2(b), (e) show that an embedded Cu-nanomesh electrode was fabricated when 2 bar of pressure were used. As shown in Figs. 2(c) and (f), the sample processed under 4 bar of pressure exhibited isolated metal islands inside a mesh grid because of bending of the PDMS stamp under relatively higher pressure.

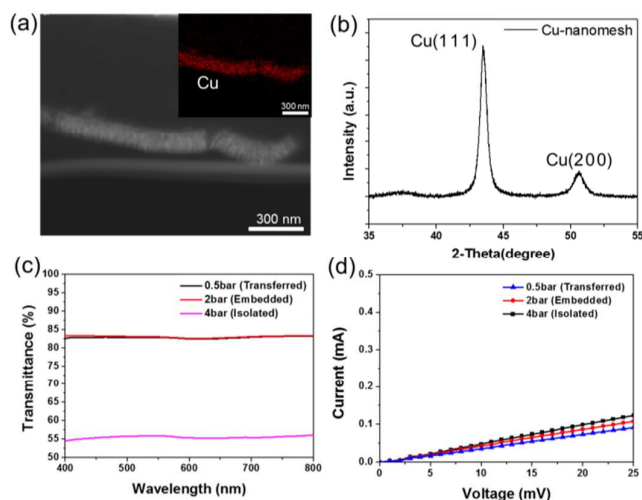


**Figure 3.** (a) HAADF-STEM cross-sectional image and EDX elemental mapping image of an embedded Cu-nanomesh electrode. (b) XRD pattern of a Cu-nanomesh. (c) Transmittance for transferred, embedded, and isolated Cu-nanomesh. (d) I-V curves of transferred, embedded, and isolated Cu-nanomesh.

As shown in Fig. 3(a), we measured the cross-sectional image of the embedded Cu-nanomesh electrode on PET substrate using a high-angle angular dark field scanning transmission electron microscope (HAADF-STEM). STEM energy-dispersive X-ray spectroscopy (EDS) mapping of the Cu electrode line indicated the spatial distribution of Cu (RED). Figure 3(b) shows the X-ray diffraction (XRD) pattern of the embedded Cu-nanomesh. The Cu-nanomesh had XRD peaks at 43.46° and 50.55°, which correspond to Cu(111) and Cu(200). In Fig. 3(c), the optical transmittance values of the transferred and embedded Cu-nanomesh patterns on PET are similar at around 83–84% over the wavelength range from 400 to 800 nm, but the isolated Cu-nanomesh electrode had a transmittance value of around 55% because of the isolated Cu islands inside the mesh grid. As shown in Fig. 3(d), we measured the current-voltage relationship of transferred, embedded and isolated Cu-nanomesh electrodes. It was confirmed that the value of the sheet resistance of Cu-nanomesh electrodes is very low due to the surface oxidation of Cu during the transfer process. In order to prevent surface oxidation and to obtain higher electrical conductivity, we fabricated a Cu/Au-nanomesh to replace the Cu-nanomesh pattern.

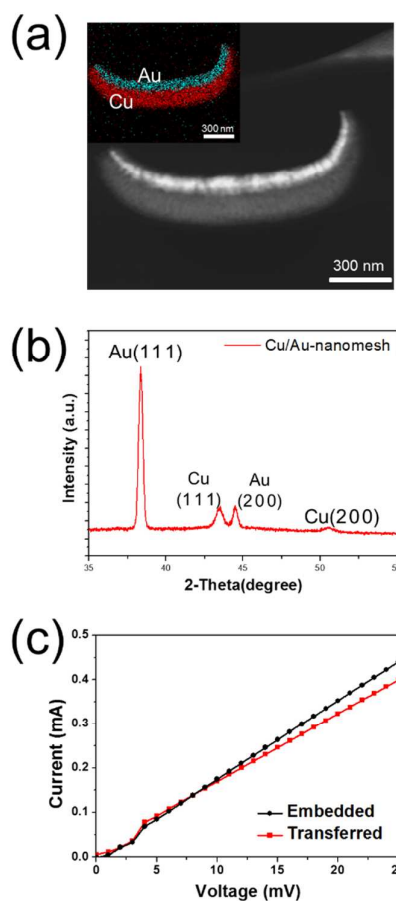


**Figure 4.** (a) HAADF-STEM cross-sectional image and EDX elemental mapping image of embedded Cu/Au-nanomesh electrodes. (b) XRD pattern of a Cu-nanomesh. (c) I-V curves of transferred, embedded, and isolated Cu/Au-nanomesh.

In order to form the Cu/Au bilayer-nanomesh structure, 50 nm of Au were deposited on the PDMS stamp before Cu deposition on the PDMS mold. Then, 100 nm of Cu were deposited. As shown in Fig. 4(a), we confirmed the cross-sectional image of the embedded Cu/Au-nanomesh electrode using HAADF-STEM. An EDS mapping of the Cu/Au electrode line indicated the spatial distribution of Cu (red) and Au (magenta). Figure 4(b) shows the X-ray diffraction (XRD) pattern of the embedded Cu/Au-nanomesh. The Cu/Au-nanomesh had XRD peaks at 38.33°, 44.49°, 43.46°, and 50.55°, which indicated Au(111), Au(200), Cu(111), and Cu(200) simultaneously. Because of the unchanging mesh pattern size and array, the Cu/Au-nanomesh had the same transmittance as the Cu-nanomesh electrode, which was 83% over the wavelength range from 400 to 800 nm. According to Fig. 4(c), the sheet resistance value of the Cu/Au-nanomesh was one fifth that of the Cu-nanomesh. It is believed that the Au layer on the Cu layer prevented the oxidation of the Cu surface during the heating and pressing process. Consequently, high values of optical transmittance and electrical conductivity were obtained for the Cu/Au-nanomesh structure.

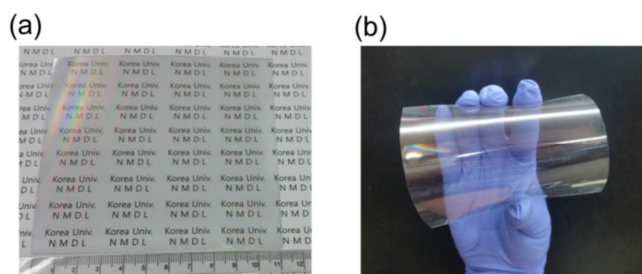


**Figure 5.** (a) Photograph of the Cu/Au-nanomesh on a PET substrate. (b) Photograph of a flexible Cu/Au-nanomesh electrode.

Figure 5 shows photographs of the Cu/Au-nanomesh pattern on a PET film. The sample was very transparent and could be easily rolled. The size of sample was up to 110 mm x 110 mm.

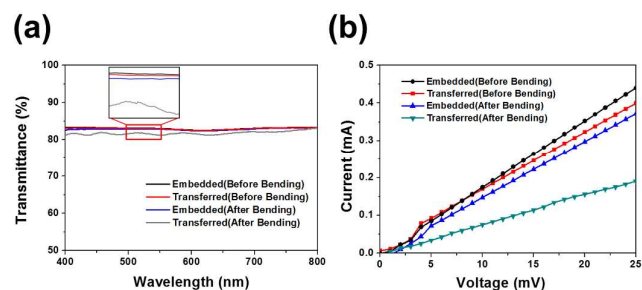


**Fig. 6.** Variation in the (a) optical transmittance and (b) electrical conductivity of Cu-nanomesh patterns after 50,000 bending cycles.

Figure 6 shows the transmittance and sheet resistance of the transferred and embedded Cu/Au-nanomesh electrodes, which were measured after 50,000 bending cycles. The optical transmittance of the embedded Cu/Au-nanomesh electrode did not degraded with bending. However, a slight decrease in the optical transmittance was observed for the transferred Cu/Au-nanomesh electrode. The electrical conductivity decreased slightly for both embedded and transferred Cu/Au-nanomesh electrodes because of the mechanical stress build-up in the metal structure during bending. In this case, the decrease in the electrical conductivity of the embedded Cu/Au-nanomesh electrode was less severe than that of the transferred Cu/Au-nanomesh electrode. Even after 50,000 bending cycles, the embedded Cu/Au-nanomesh electrode maintained its optical transmittance and electrical properties because the embedded Cu/Au-nanomesh pattern was strongly adhered on the polymer PET film.

Although ITO has a high optical transparency and electrical conductivity, its application is limited by its high cost, brittleness, and susceptibility to conductivity changes if subject to bending. However, transparent embedded Cu/Au-nanomesh electrodes could replace ITO electrodes because of their high optical and electrical properties and stability.

The optical and electrical properties of Cu/Au-nanomesh electrodes must be enhanced in comparison with those of ITO, AZO, and FTO electrodes. To overcome the limitations of Cu/Au-nanomesh electrodes, hybrid Cu/Au-nanomesh and ITO electrodes have the advantages of stable optical and electrical properties. Cu/Au-nanomesh electrodes can enhance the efficiency of conducting electrodes in optoelectronic devices, such as LEDs, LCDs, OLEDs, and photovoltaic devices.

#### 4. Conclusions

A Cu/Au-nanomesh electrode structure was fabricated over a PET flexible polymer film using a transfer process. By adjusting the printing pressure, the metal-nanomesh could be embedded into a polymer film. During the printing process, the Cu surface was oxidized, which resulted in a decrease in the electrical conductivity. By replacing the Cu layer with a Cu/Au bilayer, Cu oxidation was prevented, and a high electrical conductivity was obtained.

Compared to the transferred nanomesh electrode, the embedded electrode exhibited improved optical transmittance and electrical conductivity. Moreover, the properties of the embedded electrode were maintained after 50,000 bending cycles. Thus, it is an appropriate choice for flexible transparent electrodes.

#### Acknowledgements

This research was supported by the Pioneer Research Center Program through the National Research Foundation of Korea funded by the Ministry of Science, ICT & Future Planning (NRF-2013M3C1A3063597). This research was supported by the Nano-Material Technology Development Program through the National Research Foundation of Korea (NRF) funded by the Ministry of Education, Science, and Technology (2012M3A7B4035323).

#### Notes and references

- 1 S. Park, G. Wang, B. Cho, Y. Kim, S. Song, Y. Ji, M.-H. Yoon, and T. Lee, *Nat. Nanotechnol.*, 2012, **7**, 438.
- 2 T.-H. Han, Y. Lee, M.-R. Choi, S.-H. Woo, S.-H. Bae, B. H. Hong, J.-H. Ahn, and T.-W. Lee, *Nat. Photonics*, 2012, **6**, 105.
- 3 S. E. Shaheen, C. J. Brabec, N. S. Sariciftci, F. Padinger, T. Fromherz, and J. C. Hummelen, *Appl. Phys. Lett.*, 2001, **78**, 841.
- 4 G. Li, V. Shrotriya, J. S. Huang, Y. Yao, T. Moriarty, K. Emery, and Y. Yang, *Nat. Mater.*, 2005, **4**, 864.
- 5 Y. B. Yuan, Y. Bi, and J. S. Huang, *Appl. Phys. Lett.*, 2011, **98**, 063306.
- 6 X. Y. Zeng, Q. K. Zhang, R. M. Yu and C. Z. Lu, *Adv. Mater.*, 2010, **22**, 4484.
- 7 C. C. Wu, C. I. Wu, J. C. Sturm, and A. Kahn, *Appl. Phys. Lett.*, 1997, **70**, 1348.
- 8 H. Kim, C. M. Gilmore, A. Pique, J. S. Horwitz, H. Mattoussi, H. Murata, Z. H. Kafafi, and D. B. Chrisey, *J. Appl. Phys.*, 1999, **86**, 6451.

- 9 H. Kim, A. Pique, J. S. Horwitz, H. Mattoussi, H. Murata, Z. H. Kafafi, and D. B. Chrisey, *Appl. Phys. Lett.*, 1999, **74**, 3444.
- 10 H. Kim, C. M. Gilmore, J. S. Horwitz, A. Pique, H. Murata, G. P. Kushto, R. Schlaf, Z. H. Kafafi, and D. B. Chrisey, *Appl. Phys. Lett.*, 2000, **76**, 259.
- 11 X. Jiang, F. L. Wong, M. K. Fung, and S. T. Lee, *Appl. Phys. Lett.*, 2003, **83**, 1875.
- 12 X. T. Hao, L. W. Tan, K. S. Ong, and F. R. Zhu, *J. Cryst. Growth*, 2006, **287**, 44.
- 13 K. Fehse, K. Walzer, K. Leo, W. Lövenich, and A. Elschner, *Adv. Mater.*, 2007, **19**, 441.
- 14 D. R. Cairns, R. P. Witte li, D. K. Sparacin, S. M. Sachsman, D. C. Paine, G. P. Crawford, and R. R. Newton, *Appl. Phys. Lett.*, 200, **76**, 1425.
- 15 Y. M. Chang, L. Wang, and W. F. Su, *Org. Electron.*, 2008, **9**, 968.
- 16 S. I. Na, S. S. Kim, J. Jo, and D. Y. Kim, *Adv. Mater.*, 2008, **20**, 4061.
- 17 M. L. Machala, L. Muller-Meskamp, S. Gang, S. Olthof, and K. Leo, *Org. Electron.*, 2011, **12**, 1518.
- 18 M. W. Rowell, M. A. Topinka, M. D. McGehee, H. J. Prall, G. Dennler, N. S. Sariciftci, L. B. Hu, and G. Gruner, *Appl. Phys. Lett.*, 2006, **88**, 233506.
- 19 T. M. Barnes, J. D. Bergeson, R. C. Tenent, B. A. Larsen, G. Teeter, K. M. Jones, J. L. Blackburn, and J. van de Lagemaat, *Appl. Phys. Lett.*, 2010, **96**, 243309.
- 20 S. Kim, J. Yim, X. Wang, D. D. C. Bradley, S. Lee, and J. C. Demello, *Adv. Funct. Mater.*, 2010, **20**, 2310.
- 21 K. S. Kim, Y. Zhao, H. Jang, S. Y. Lee, J. M. Kim, J. H. Ahn, P. Kim, J. Y. Choi, and B. H. Hong, *Nature*, 2009, **457**, 706.
- 22 S. Bae, H. Kim, Y. Lee, X. F. Xu, J. S. Park, Y. Zheng, J. Balakrishnan, T. Lei, H. R. Kim, Y. I. Song, Y. J. Kim, K. S. Kim, B. Ozyilmaz, J. H. Ahn, B. H. Hong, and S. Iijima, *Nat. Nanotechnol.*, 2010, **5**, 574.
- 23 H. Wu, L. B. Hu, M. W. Rowell, D. S. Kong, J. J. Cha, J. R. McDonough, J. Zhu, Y. A. Yang, M. D. McGehee, and Y. Cui, *Nano Lett.*, 2010, **10**, 4242.
- 24 D. S. Hecht, L. B. Hu, and G. Irvin, *Adv. Mater.*, 2011, **23**, 1482.
- 25 M. W. Rowell, M. A. Topinka, M. D. McGehee, H. J. Prall, G. Dennler, N. S. Sariciftci, L. B. Hu, and G. Gruner, *Appl. Phys. Lett.*, 2006, **88**, 233506.
- 26 S. Kim, J. Yim, X. Wang, D. D. C. Bradley, S. Lee, and J. C. Demello, *Adv. Funct. Mater.*, 2010, **20**, 2310.
- 27 Q. Y. He, H. G. Sudibya, Z. Y. Yin, S. X. Wu, H. Li, F. Boey, W. Huang, P. Chen, and H. Zhang, *ACS Nano*, 2010, **4**, 3201.
- 28 Z. Y. Yin, S. Y. Sun, T. Salim, S. X. Wu, X. A. Huang, Q. Y. He, Y. M. Lam, and H. Zhang, *ACS Nano*, 2010, **4**, 5263.
- 29 G. Eda, G. Fanchini, and M. Chhowalla, *Nat. Nanotechnol.*, 2008, **3**, 270.
- 30 S. Coskun, E. S. Ates, and H. E. Unalan, *Nanotechnology*, 2013, **24**, 125202.
- 31 H.-J. Choi, S. Choo, P.-H. Jung, J.-H. Shin, Y.-D. Kim and H. Lee, *Nanotechnology*, 2015, **26**, 055305.
- 32 Y. Xia and G. M. Whitesides, *Annu. Rev. Mater. Sci.*, 1998, **28**, 153.